Ionospheric ions in the near-Earth magnetotail

Sheng-Hsien Chen[1] and Thomas E. Moore[2]

Received 14 September 2007; revised 1 April 2008; accepted 2 May 2008; published 30 August 2008.

[1] We report studies of the relationship between geomagnetic storms and the spatial distribution of cold ions, mostly of ionospheric origin, in the near-Earth magnetotail using in situ particle and field measurements from the Polar spacecraft, solar wind measurements from the ACE spacecraft, and ground geomagnetic indices, during the years from 2000 to 2005. We find local time and latitude-dependent distributions of the plasma moments of cold ions at various levels of geomagnetic storms characterized by the Sym-H and Dst indices. (1) Denser cold ions were observed at the duskside ($N > 10$ cm^{-3} compared with 1 cm^{-3} on average): consistent with the formation of plasma plumes and enhanced bulge region formed as the cold ions wrapped under corotation. (2) Higher temperatures were observed in the auroral oval regions, and a larger temperature anisotropy was observed at the dawnside. (3) Heating processes were strongest near midnight and in the auroral oval regions, which map to PSBL or CPS, except during extremely high geomagnetic activity levels, when heating occurred at high latitudes toward the dawnside, which map to the plasma mantle or distant magnetotail. We interpret these variations as results of ionospheric outflows and plasmaspheric expansion interacting with enhancements of near-Earth magnetospheric convection and geomagnetic-storm-related heating processes in the magnetotail.

Citation: Chen, S.-H., and T. E. Moore (2008), Ionospheric ions in the near-Earth magnetotail, *J. Geophys. Res.*, *113*, A08232, doi:10.1029/2007JA012816.

1. Introduction

[2] Large-scale expansion of the ionosphere by storm-induced electric fields produces massive ion flows into the magnetosphere. An enhanced polar wind, including heavy-ion plasmas from the low-altitude cusp and auroral regions, and erosion of plasmasphere, are all consequences of large-scale ionospheric changes that are especially prevalent during intense storms. These ionospheric ions populate the ring current and plasma sheet, and interact with the solar wind plasma in the outer magnetospheric boundary layers, and thereby, couple back into ionospheric plasma electrodynamics. Evidence of the ionospheric ions in the outer magnetosphere has been abundant [*Young et al.*, 1977; *Roux et al.*, 1982; *Chappell et al.*, 1987; *Farrugia et al.*, 1989; *Mukai et al.*, 1994; *Wilken et al.*, 1995; *Hirahara et al.*, 1996; *Seki et al.*, 1998]. Their level of importance increased further recently with new analyses based on measurements from Polar, IMAGE, and Cluster spacecraft [*Marcucci et al.*, 2004; *Chen and Moore*, 2004, 2006; *Ohtani et al.*, 2006]. These analyses reinforce older findings that the cold ionospheric ions of few tens of eV in energy, with negligible thermal pressure, become a dominant plasma component, denser than protons, during storm-time, after being dramatically heated and dynamically involved in the magnetospheric processes at various scales. The detections of keV O^+ abundant near the geosynchronous orbit [*Fritz and Wilken*, 1976; *Lavraud et al.*, 2005], in the outer magnetosphere [*Shelley et al.*, 1974; *Geiss et al.*, 1978; *Young*, 1979], in the lobes [*Candidi et al.*, 1982; *Seki et al.*, 1998], plasma sheet [*Wilken et al.*, 1995; *Ruan et al.*, 2005], low-latitude boundary layers [*Chaston et al.*, 2005], and in the magnetosheath [*Marcucci et al.*, 2004] are among the examples of this.

[3] Storm-time global distributions of cold ions are particularly important in terms of how the sources and sinks of cold ionospheric ions might be located and involved in the global dynamics at various level of geomagnetic activity. *Chen and Moore* [2006] have shown that the spatial distributions of cold ions and their convection in the dayside magnetosphere is a function of the orientation of interplanetary magnetic field (IMF), which controls the magnetic reconnection rate at the dayside. They concluded that the extent of cold ions is significantly expanded both radially and in local time during southward IMF, as compared with that which prevails during northward IMF. Particularly at the duskside this expansion, known as the extension of plasmasphere or plasma plume, could reach the dayside magnetopause during strong sunward convection. On the nightside, the reconfiguration of the magnetosphere because of geomagnetic activity is much more complex on the dayside. The energy releases and recovery of the magnetosphere to its quiet state are processes involving magnetotail reconnection processes, and these are delayed in the near-Earth magnetotail. As a result, a more direct and violent interchange of plasmas between the plasma

[1]USRA and Geospace Physics Laboratory, Heliophysics Science Division, NASA Goddard Space Flight Center, Greenbelt, Maryland, USA.
[2]Heliophysics Science Division, NASA Goddard Space Flight Center, Greenbelt, Maryland, USA.

Copyright 2008 by the American Geophysical Union.
0148-0227/08/2007JA012816

sheet and the ionosphere might occur in this region. Spatially distinctive current disruptions, reconnection in the plasma sheet, and corresponding auroral processes in the ionosphere are the manifestation of these processes occurring during geomagnetic storms or substorms. Knowledge of the spatial distributions of cold ions in the magnetotail at various levels of geomagnetic activity is an important prerequisite to understanding how these ionospheric ions might contribute to storms or substorm dynamics.

[4] Here we provide a quantitative study of the global distributions of ionospheric ions in the near-Earth magnetotail, and their evolution with levels of geomagnetic activity. We analyzed six years of Polar cold ion and magnetic field measurements in 1-min resolutions when the spacecraft was in the nightside. We used 1-min resolution Sym-H index, instead of 1-hour resolution Dst, as the indicator of the levels of geomagnetic activity, particularly for global geomagnetic storms that create disturbances in the intensity of ring current. We will show the correlation with Sym-H and Dst and discuss their similarities and differences. We will describe how the data were collected and processed first and then present results in terms of spatial distributions of the plasma moments, density, temperatures and velocity, and a special quantity representing the heating ratio of cold ions at various levels of geomagnetic activity. We elaborate the results and discuss their implications in the discussion section, followed by the conclusions.

2. Data

[5] We used in situ measurements of cold ions and magnetic field from Thermal Ion Dynamics Experiment (TIDE) [*Moore et al.*, 1995] and MFE [*Russell et al.*, 1995] instruments, respectively, on the Polar spacecraft collected between the years of 2000 and 2005. We calculated the plasma moments of Thermal Ion Dynamics Experiment (TIDE) including ion density, temperature and velocity at 1-min resolution for the periods of July to November of each year, when Polar was in the nightside between 5 and 9 R_E. The orbital coverage is shown in GSM coordinate in Figure 1. There was good nightside coverage in local time near the equator ($Z_{GSM} = 0$) but less so at higher latitudes either to the north or south toward the dawnside or duskside (Figure 1c). The ground traces, mapped from the Polar orbits using the Tsyganenko 96 external magnetic field model [*Tsyganenko*, 1995] and the up-to-date International Geomagnetic Reference Field (IGRF) internal magnetic field model, are shown in Figure 2. The ground traces in the northern (southern) polar cap were started from where the measurement of B_x is positive (negative). We used corrected magnetic coordinates; that is, invariant latitude versus magnetic local time based on the field models, to organize our data set and to represent the 3-D spatial distributions of the plasma moments in 2-D. We then merged Polar data with the Sym-H index [*Iyemori*, 1990]. Sym-H, from ground magnetic field perturbations of ten mid-latitude stations around the globe, can be used as a proxy for Dst index [*Sugiura and Poros*, 1971], which is an indicator of the level of enhancements in the ring current at global geomagnetic storm times, with the advantage of higher time resolution of 1-min over the typical 1-hour Dst [*Iyemori and Rao*, 1996; *Wanliss and Showalter*, 2006]. To validate, we analyzed the correlations between Sym-H at 1-hour resolution and Dst indices for our data set. Figure 3 shows the linear least-squares fits for (1) minimizing Dst, (2) minimizing Sym-H, and (3) the best fit based on the two methods. The correlation coefficients of the best fits are 0.976 (Figure 3a) and 0.949 (Figure 3b) for the Dst ranges of [200, −600] and [200, −200], respectively. The correlations are good except that there are significantly deviated Sym-H clusters of distributions in the Dst range of [0, −80] that might indicate more subtle variations in the Earth current systems where the Sym-H stations was located.

3. Analyses

[6] To understand how the cold ionospheric plasmas in the near-Earth magnetotail are distributed during geomagnetic storms, we calculated the plasma moments including density, temperature and velocity and classified them into four levels of geomagnetic activity characterized by Sym-H, namely the quiet (Sym-H > −10), weakly disturbed (−10 > Sym-H >−30), moderately disturbed (−60 > Sym-H > −30), highly disturbed (Sym-H < −60). We plotted the data as two-dimensional contours in magnetic coordinate which trace back to the ground, i.e., for each location where the plasma moments were calculated, we traced its footprint on the ground along magnetic field lines in a way as described in the previous section. For each average taken in a 5° invariant-latitude by 1-hour local-time bin, we required the number of orbits in each bin to be 10 or more; otherwise we treated it as a data gap.

[7] Figure 4 shows the two-dimensional density contours in magnetic local time in hours versus invariant latitude in degrees for the four levels of geomagnetic activity characterized by Sym-H. The density contours are color-coded at levels of base-ten logarithmic values (cm^{-3}) indicated at the right of Figures 4a and 4c. Model auroral ovals [*Holzworth and Meng*, 1975] at the corresponding levels of geomagnetic activity are overlaid (dashed curves). On average, the number densities were on the orders of 0.2 to 0.6 and 2 to 10 cm^{-3} in the northern and southern hemispheres, respectively. The densities in the southern hemisphere were significantly higher. While there are many possibilities that could cause the north–south ion density asymmetry in the magnetotail, we suggest, and provide preliminary tests showing that this results from seasonal biases in our database, which provided more summer and autumn data (all in July – November but none in December–June) when the Earth's dipole titled toward the Sun and created conditions favorable for cold ionospheric ions filling the magnetotail. We have tested the summer and autumn subsets for the north–south asymmetries, but did not find a statistically significant modification of the degree of asymmetry, because significantly more data gaps were introduced. We need exclusively spring or winter measurements to verify this, but this is not possible since Polar was in the dayside magnetosphere during these times. We have also tested the magnetic field fluxes in our database to see whether the density asymmetries attribute to the magnetic field stress balance between the northern and southern lobes. Figure 5 shows the contours for magnetic field strength as a function of geomagnetic activity levels. It shows that there were north–south asymmetries in the

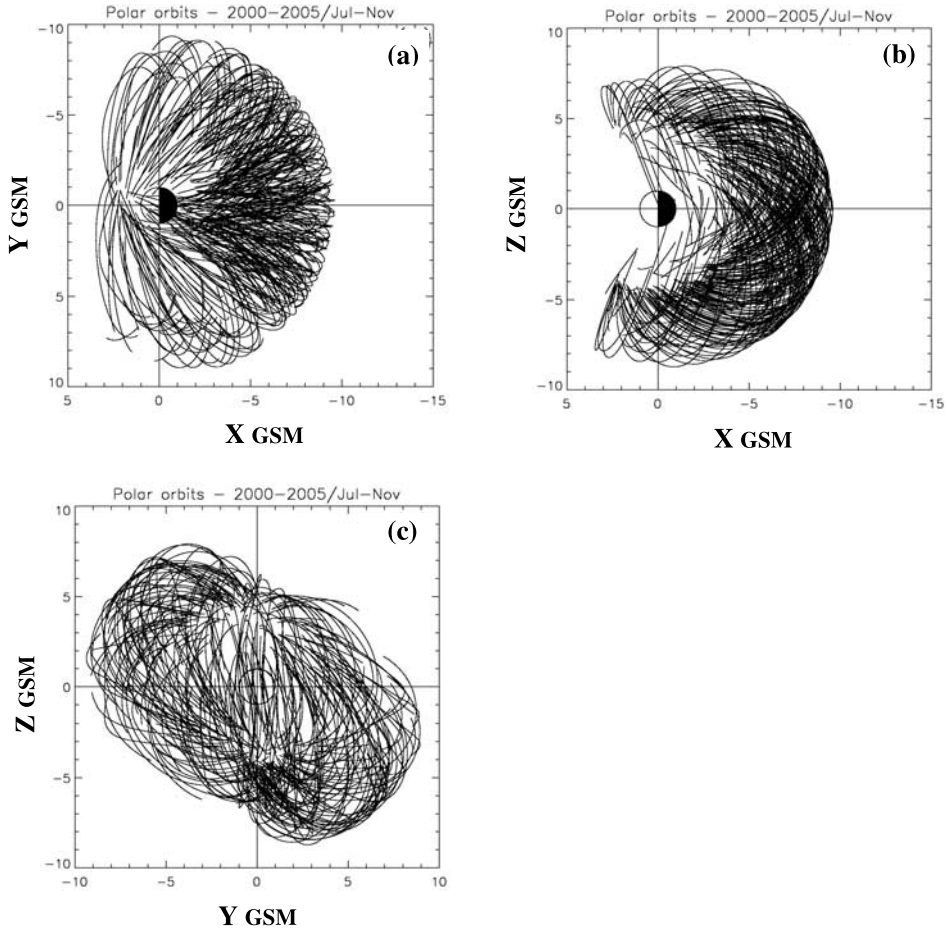

Figure 1. Traces of Polar apogee-half orbits (r > 5 R_E) for the periods of July to November of the years 2000 to 2005. Only every five orbits are plotted. (a) X–Y_{GSM} plane, (b) X–Z_{GSM} plane, and (c) Y–Z_{GSM} plane.

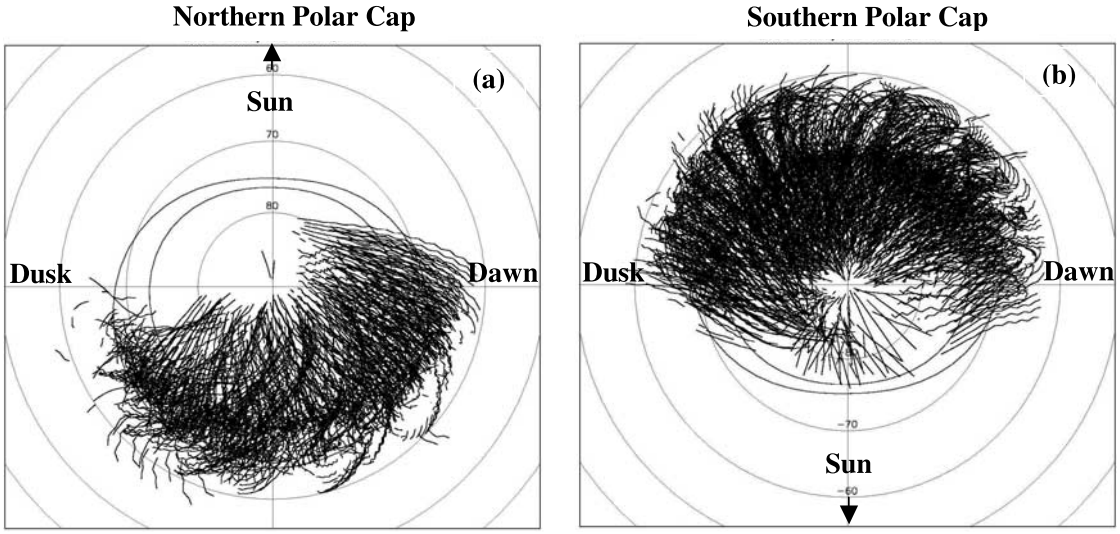

Figure 2. Ground traces of Polar apogee-half orbits for the periods of July to November of the years 2000 to 2005. Tsyganenko 96 external magnetic field [*Tsyganenko*, 1995] with the latest IGRF internal field model for the years was used to map from the orbits to the ground. Model auroral ovals [*Holzworth and Meng*, 1975] for medium geomagnetic activity were overlaid. (a) Mapping in northern hemisphere that look from above, Sun at the top. (b) Mapping in the southern hemisphere that look from below, Sun at the bottom keeping the dawn–dusk direction the same as Figure 2a.

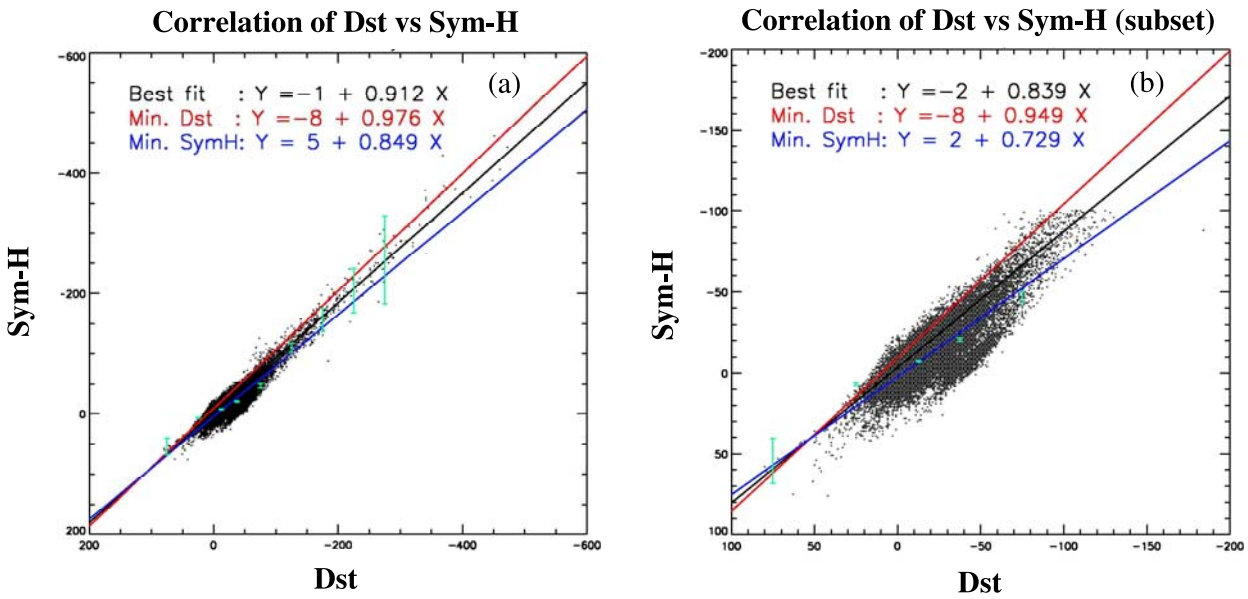

Figure 3. Correlations between Sym-H at 1-hour resolution and Dst indices for the data set used in this study. Figures 3a and 3b are for the full-set Dst range [200, −600] and the subset [200, −200], respectively. Standard error bars are also shown.

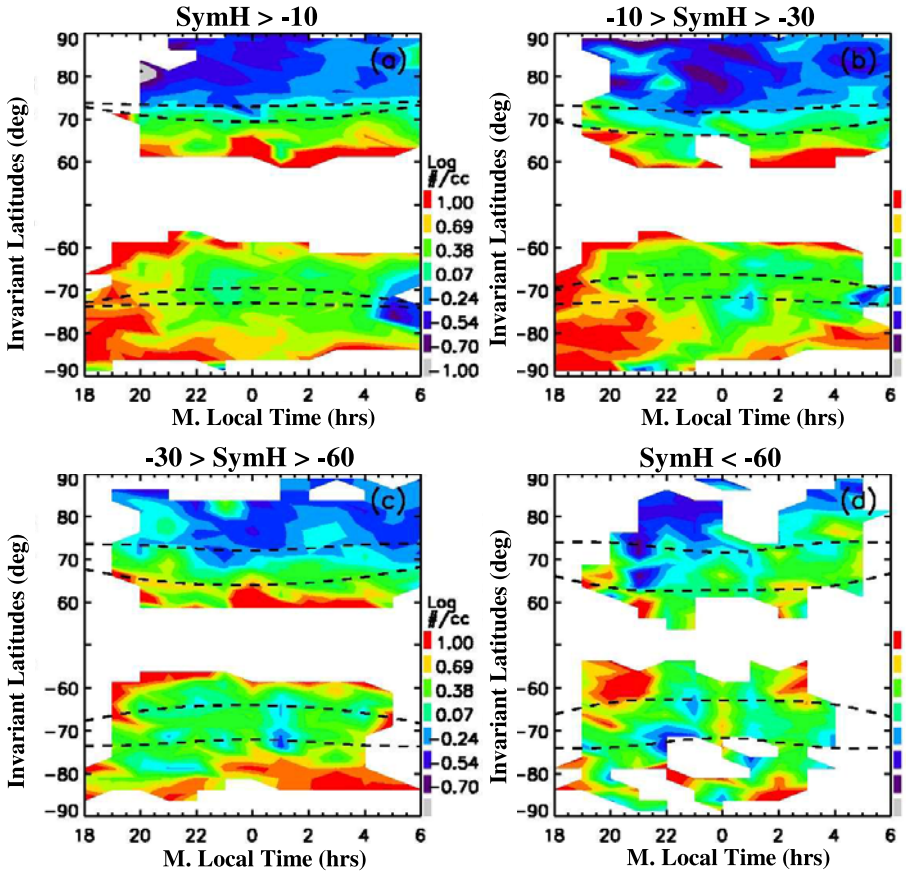

Figure 4. Two-dimensional density contours in magnetic local time (hours) versus invariant latitude (degrees) for four levels of geomagnetic activity characterized by Sym-H. The density contours are color-coded at levels of ten-based logarithmic values in cm^{-3} shown to the rights of Figures 4a and 4c. Model auroral ovals [*Holzworth and Meng*, 1975] at the corresponding levels of geomagnetic activity are overlaid (dashed curves).

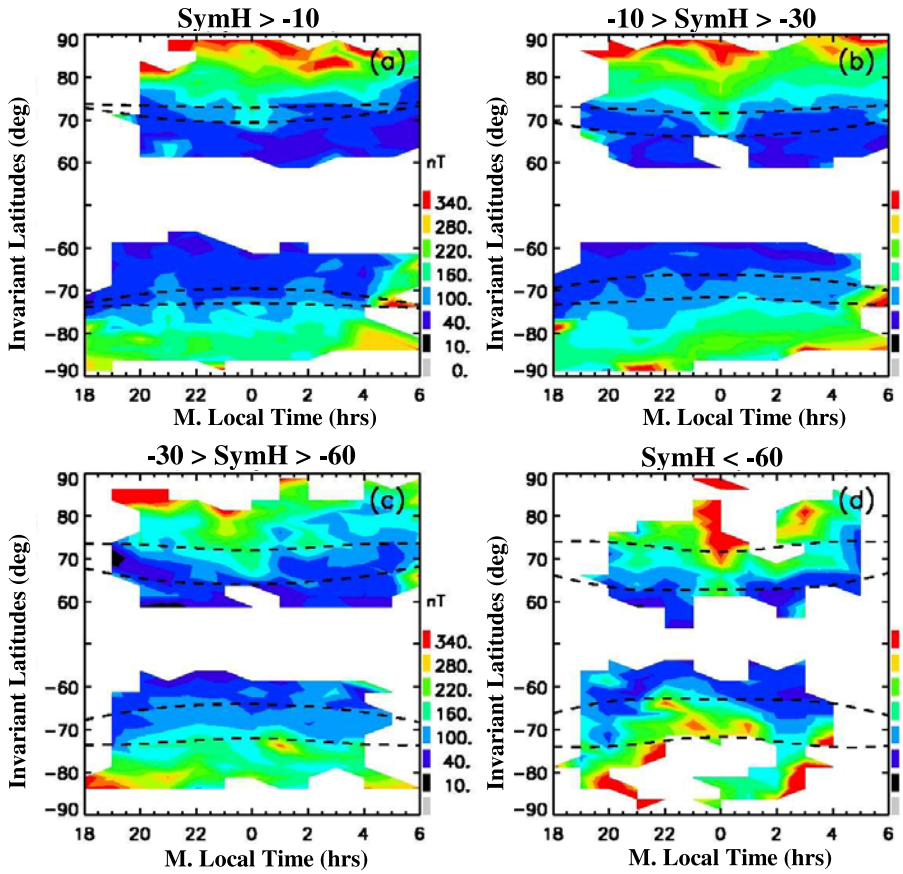

Figure 5. Contours of magnetic field magnitude at various levels of geomagnetic activity. The format and classification of geomagnetic activity are the same as Figure 3.

magnetic field. The magnetic fields were stronger in the northern hemisphere than in the southern hemisphere at corresponding latitudes, but this was less clear at the extreme geomagnetic activity when larger data gaps enhanced the uncertainties.

[8] We offer two physical processes as illustrated in Figure 6 to interpret the above. Firstly, Polar was detecting lower ion fluxes in the northern lobes, in which the magnetic fields were relatively more compressed than in the southern lobes owing to the more northward position of the neutral sheet for dipole tilt of the north pole toward the sun (zero tilt position is indicated by the dashed line). Secondly, the region favorable for dayside magnetic reconnection, associated with a southward component in the IMF,

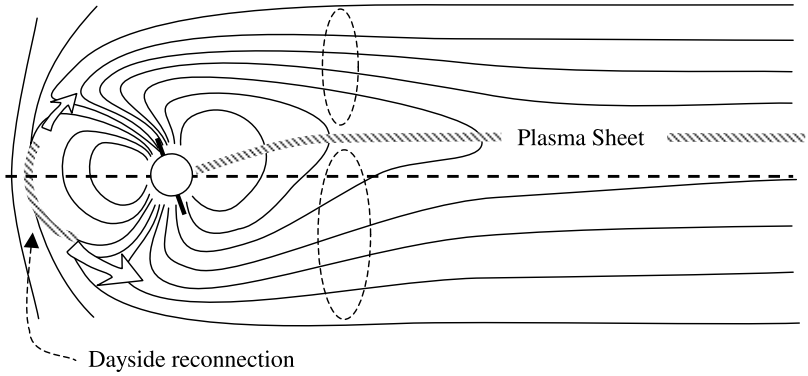

Figure 6. A schematic to explain the north–south asymmetries in densities and magnetic field strength. When the dipole axis is tilting toward the sun, the magnetic field in the northern lobe is more compressed than in the southern lobe. At dayside, the accumulated tailward flux in the southern hemisphere caused by reconnection is higher than in the northern hemisphere. The schematic is an abstraction of the empirical models of the positions of dayside high-latitude magnetopause and polar cusps of *Boardsen et al.* [2000] and plasma sheet of *Hammond et al.* [1994].

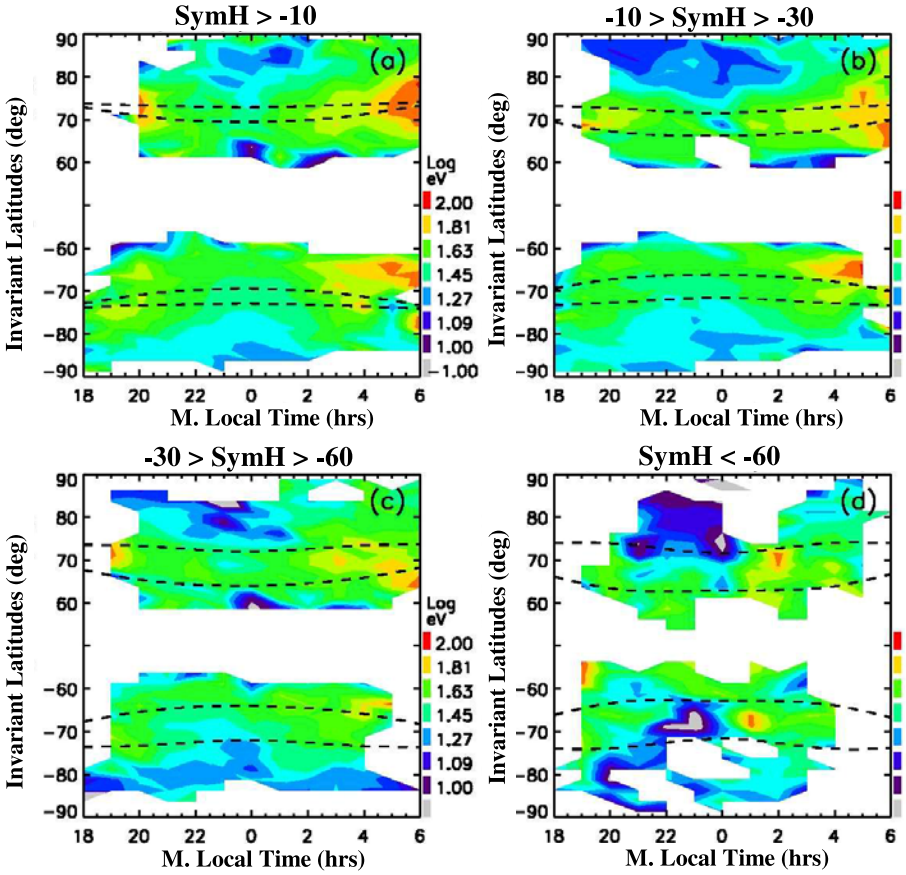

Figure 7. Same as Figure 3 but for $T_{\|}$. The contour levels are color-coded to the ten-based logarithmic values of $T_{\|}$ in electron volt.

moves into the southern hemisphere when northern magnetic pole is tilted toward the Sun [*Boardsen et al.*, 2000; *Eastman et al.*, 2000; *Trattner et al.*, 2006]. This should create stronger southward flows with higher accumulated plasmaspheric fluxes and feed the southern high-latitude boundary and the lobe. During quiet times when Sym-H > −10, and weakly disturbed times when −10 > Sym-H > −30 (Figures 4a and 4b), the densities were higher at the duskside (18–22 MLT) than at the other local times at the invariant latitudes of −70 to near −90. This is consistent with the scenario in which the plasma plumes exit the plasmasphere toward the duskside during initial phases of strong convection occurring during periods of southward IMF or major geomagnetic disturbed times [*Chen and Moore*, 2006]. These plumes could also extend to higher southern latitudes well above the auroral oval regions as shown in Figures 4a and 4b. It is interesting that the lobe fields strengthen and the plasma sheet thins when geomagnetic activity increases (Figure 6). This was more significant near midnight in the northern hemisphere where the lobe fields were thought more likely to pileup before convecting toward the plasma sheet.

[9] Figure 7 shows the 2-D contour plot of the parallel temperature $T_{\|}$ for each level of geomagnetic activity. $T_{\|}$ was in general higher at ∼30–60 eV in the auroral ovals or lower latitudes, mapped to plasma sheet boundary layer and lower at ∼10 eV in the lobes at higher latitudes. There were hot spots with $T_{\|}$ reaching 100 eV near the dawnside mostly seen during quiet (Sym-H > −10) or weakly disturbed (−10 > Sym-H > −30) time (Figures 7a and 7b). Similarly, $T_{\perp}$ was higher in the vicinities of auroral ovals but lacking the dawn–dusk asymmetries (Figure 8). The temperature isotropy $T_{\|}/T_{\perp}$, therefore, also reveals dawn–dusk asymmetries (Figure 9). $T_{\|}/T_{\perp}$could reach 2.0 at the dawnside compared with ∼1.5 at the other local times mostly during geomagnetic quiet and weakly disturbed times (Figures 9a and 9b). During highly disturbed times (Sym-H < −60), $T_{\|}/T_{\perp} \geq 2$ occurred at high latitudes and near 20 MLT in the auroral oval regions (Figure 8d). During highly disturbed times, there were noticeable patches of low $T_{\|}/T_{\perp}$ ratio at ∼0.6 between 21–24 MLT in the southern hemisphere. While $T_{\|}/T_{\perp}$ in the magnetotail was in general hotter along the magnetic field lines, there were patches of isotropic temperature at localized regions at various levels of geomagnetic activity. Several physical processes might apply. The higher $T_{\|}/T_{\perp}$ ratios at the dawnside coincide with higher Pc 5 wave activity prevailing in the plasma and magnetic field data - stronger wave-particle interactions that coupled the waves with ionospheric outflows or precipitations. The higher $T_{\|}/T_{\perp}$ ratios but lower $T_{\|}$ or $T_{\perp}$ at high latitudes during highly disturbed times (c.f., Figures 7d, 8d, and 9d) might indicate stronger streaming of colder ions fluxes along the magnetic field lines when the magnetotail was highly disturbed. Or the high and low $T_{\|}/T_{\perp}$ratios in the auroral oval regions, confined to particular local time sectors, might indicate the strong coupling of cold ions with the current systems that couple the ionosphere and the plasma sheet boundary layers.

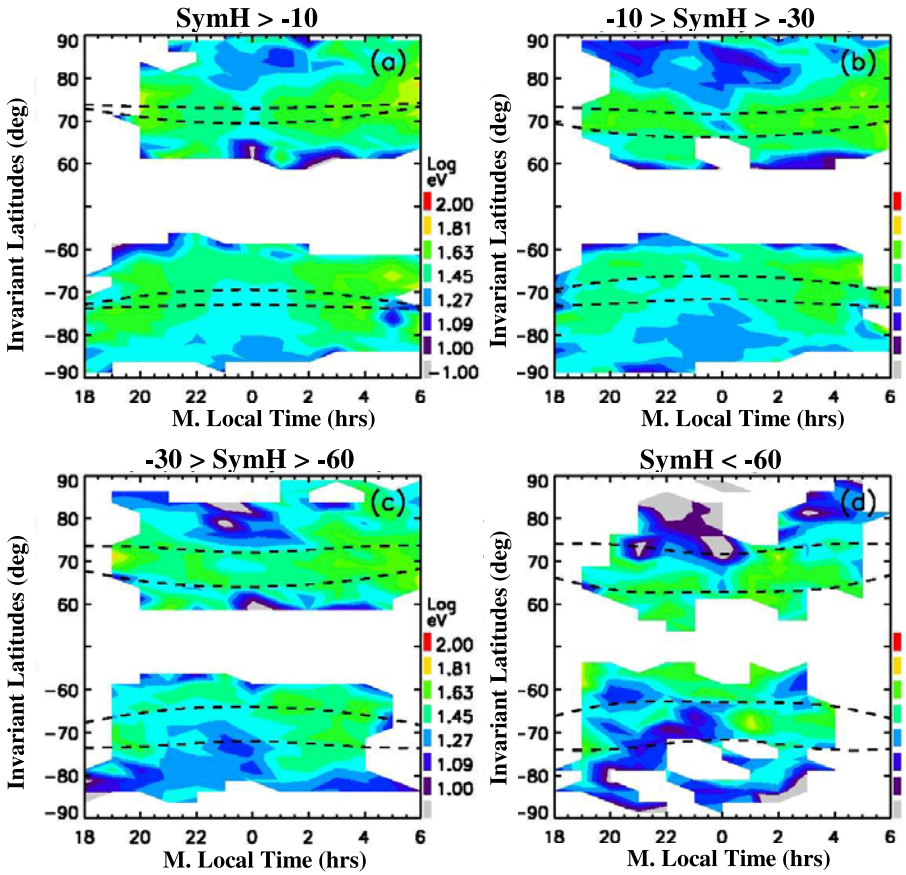

Figure 8. Same as Figure 3 but for $T_\perp$. The contour levels are color-coded to the ten-based logarithmic values of $T_\perp$ in electron volt.

[10] The parallel temperature $T_\parallel$ seems to play a role in magnetotail dynamics as more anisotropic distributions are revealed. We further examined the distribution functions close to the magnetic field lines for field-aligned anisotropy. We calculated the partial temperature along or opposite to the field line direction by integrating the distribution functions over only $\leq 45°$ parallel or anti-parallel to the field lines (Figure 10). We assigned the partial temperature as Earth-ward $T_{\text{Earthward}}$ (equation (1)) and tail-ward T_{Tailward} (equation (2)) when the integrations were performed at the earthward side and tailward side, respectively. The parallel temperature asymmetric ratio, R_A, is defined as the ratio of the two (equation (3)).

$$T_{\text{Earthward}} = G_{\nu_\theta} \sum_{\nu_\phi}^{-45<\phi<45} \sum_{\nu_r} (\nu_r - V_r)(\nu_\phi - V_\phi) f(\nu) \Delta\nu_r \Delta\nu_\phi \tag{1}$$

$$T_{\text{Tailward}} = G_{\nu_\theta} \sum_{\nu_\phi}^{135<|\phi|\leq 180} \sum_{\nu_r} (\nu_r - V_r)(\nu_\phi - V_\phi) f(\nu) \Delta\nu_r \Delta\nu_\phi \tag{2}$$

$$R_A = \frac{T_{\text{Earthward}}}{T_{\text{Tailward}}} \tag{3}$$

When R_A is much larger than unity, we call it earthward heating or simply heating as cold ionospheric ions flow back to Earth with higher temperatures. Figure 11 shows the contour levels of parallel temperature asymmetric ratio, or simply the heating ratio, R_A in invariant latitudes and local times as a function of geomagnetic activity. At quiet time (Figure 11a), the regions of heating, where $\text{Log}_{10}(R_A) > 0.35$, in the northern hemisphere were scattered at higher latitudes with peaks at the dawnside and duskside, whereas in the southern hemisphere the regions were more localized near the midnight and dawnside in the auroral oval region. As the geomagnetic activity increased (Figures 11b and 11c), the regions of heating broadened in local times and latitudes. The regions of heating in the northern hemisphere became localized at lower latitudes closer to the auroral oval region near the midnight sector. At the extremes of geomagnetic activity (Figure 11d), patches of hot regions, where the heating ratio $\text{Log}_{10}(R_A) > 0.75$, emerged mostly around midnight near the auroral oval boundaries. The hot regions might indicate asymmetric distribution functions with hotter earthward tails, assuming single distribution, or warmer cold ion populations flowing toward the Earth assuming double distributions (Figure 10). We discuss further their implications in the discussion section.

[11] It is interesting to see how the magnetospheric convection pattern changes or how the magnetic fields move in the equatorial plane in response to various levels of geomagnetic activity. Assuming no parallel electric field, the plasma is frozen-in with the magnetic fields. The flow velocity of the plasma perpendicular to the magnetic field

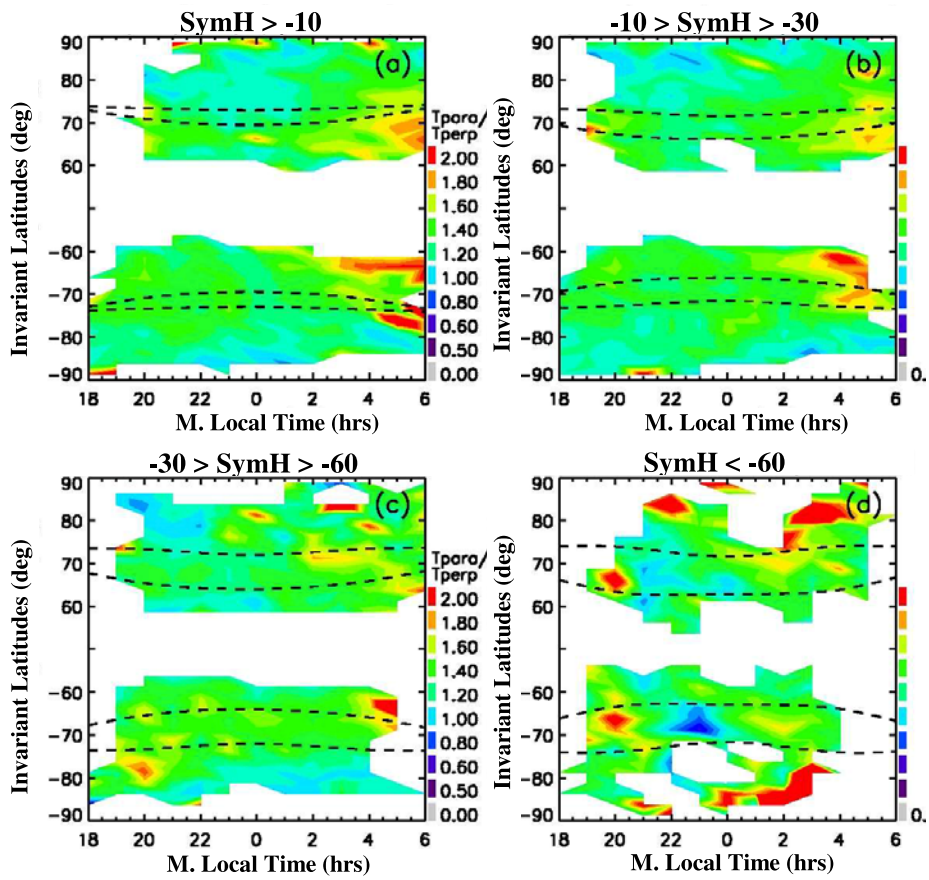

Figure 9. Same as Figure 3 but for the ratio of $T_{\parallel}/T_{\perp}$ in the linear scale.

can be treated as the convection velocity of the magnetic fields. Figure 12 shows a schematic to illustrate how the flow vectors were calculated using the cold ion measurements. The flow vectors were the averages of components taken at the regions just above and below the plasma sheet and boundary layers where the cold ions could be better measured by Thermal Ion Dynamics Experiment (TIDE) instrument. At quiet to medium geomagnetic activity (Figures 13a and 13b), flows were mostly quiet and disorganized, except small patches of eastward and earthward surges at midnight or near dawn. At higher activity (Figures 13c and 13d), flows became enhanced and turned westward in the pre-midnight sector (Figure 13d). This is consistent with the scenario of an enhanced dawn–dusk electric field to rival the corotation electric field causing sunward flows to divert around the Earth at closer distances during higher geomagnetic activity. As indicated in Figure 13d, these diverted sunward flows were observed well within the geosynchronous distance of 6.6 R_E. This is consistent with the shrinking of plasmasphere at the extreme geomagnetic activity that causes the dawn–dusk density asymmetry with the bulge of the plasmasphere moving well within 6.6 R_E and out of the scope of our data coverage, and the diminishing of plasma drainage plumes, as shown in the density distributions in Figure 4.

[12] We have provided an interpretation of the current results, but there is still considerable work to be done to confirm the hypothesis put forth in this paper. Future works to extend these analyses include the addition of other geomagnetic indices and data from other spacecraft with an expansion of the study period over a full solar cycle between 1996 and 2008. Studies of long-term solar cycle trends, as well as short-term variations of the ionospheric cold ions such as those occurring during substorm activity, are among the planned objectives of future studies.

4. Discussion

[13] The main results reported above consist of variations in the distribution of low-energy ionospheric plasmas that

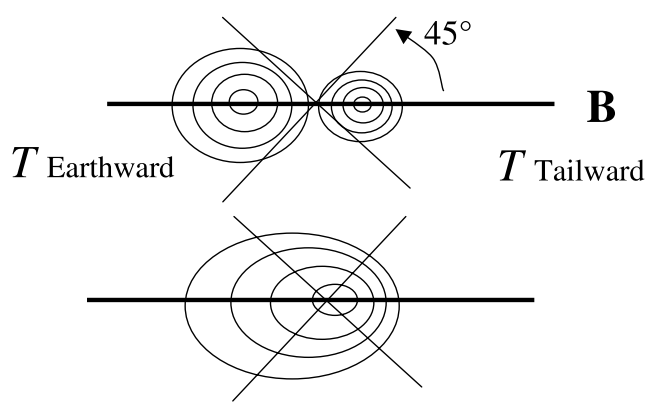

Figure 10. A schematic of how $T_{\text{Earthward}}$ and T_{Tailward} are calculated within 45° along and against the magnetic fields for two possible ion distribution functions that cause the asymmetries.

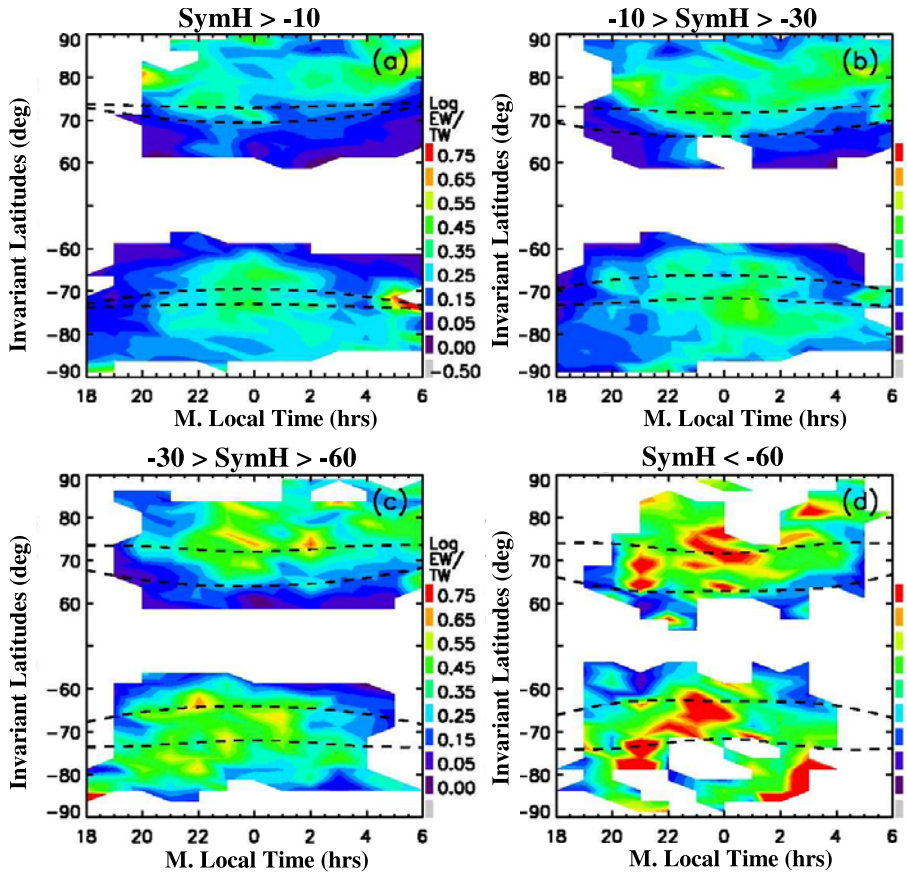

Figure 11. Same as Figure 3 but for the temperature asymmetric ratio of $R_A = T_{Earthward}/T_{Tailward}$ in ten-based logarithmic scale.

result from magnetospheric activity together with resultant changes in the circulation of plasmas flowing outward from the ionosphere. Some surprising asymmetries are also observed. We interpret the observed north–south and dawn–dusk density asymmetries (higher densities in the summer dusk southern hemisphere during lower geomagnetic activity, Figures 4a and 4b), as a manifestation of denser ionospheric outflows, reflecting the asymmetry of

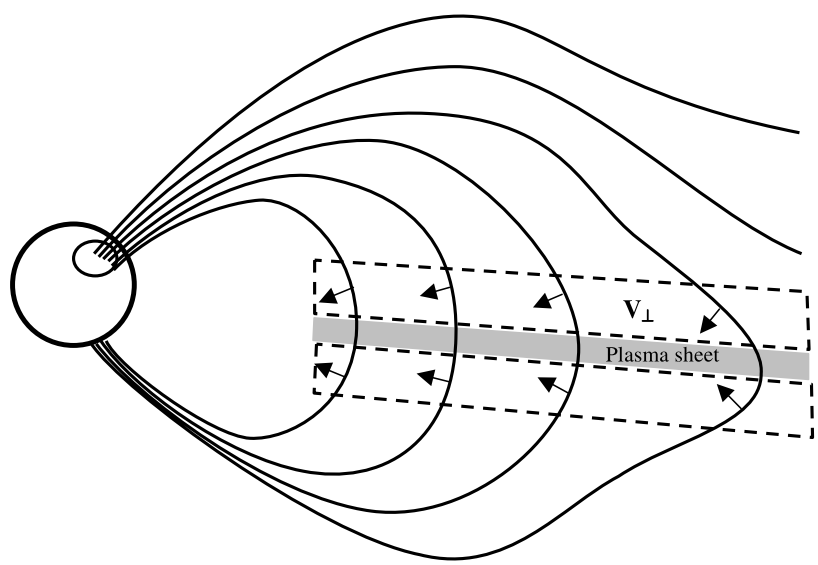

Figure 12. Schematic to illustrate how the flow vectors were calculated. The flow vectors were the averages of components taken at the regions just above and below the plasma sheet and boundary layers where the cold ions could be better measured by Thermal Ion Dynamics Experiment (TIDE) instrument.

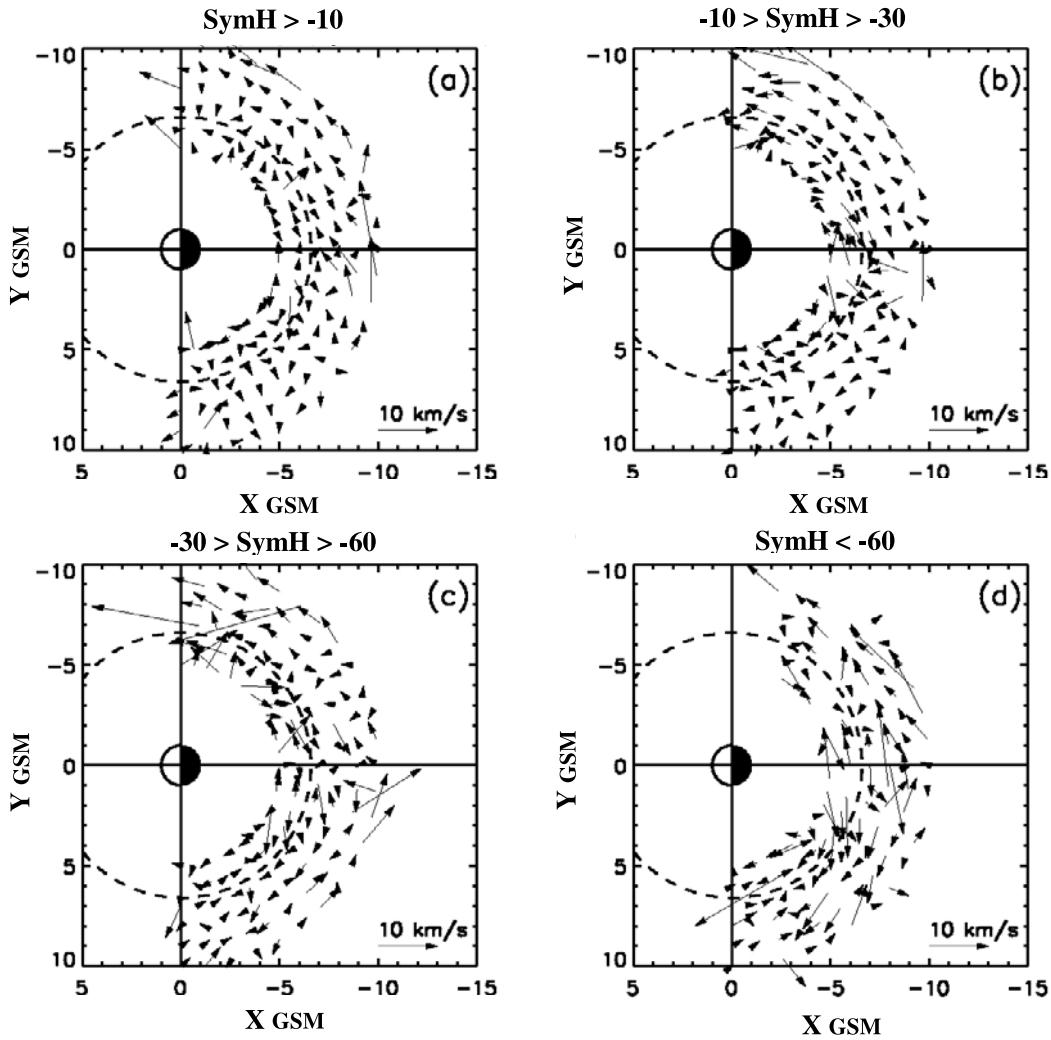

Figure 13. Velocity vectors in X–Y_{GSM} plane for levels of geomagnetic activity characterized by Sym-H.

the main body of the plasmasphere, and also affected by releases of plasma drainage plumes in earlier stages of the activity [e.g., *Goldstein et al.*, 2005]. The north–south lobe asymmetry is thought to reflect dayside reconnection region tilting into the southern hemisphere in northern summer.

[14] This interpretation is supported by the weaker magnetic intensity in the southern lobe (Figures 5a and 5b) for northern summer conditions when the plasma sheet was raised above the ecliptic plane to the north, with the locations of magnetopause boundaries axially symmetric to the X-axis [e.g., *Hammond et al.*, 1994], thereby providing a larger region into which the plasma expands. This is to be contrasted with conserving the ion flux in closed magnetic flux tubes. Contrarily, at higher geomagnetic activity (Figures 4c and 4d), the north–south asymmetries remained but the dawn–dusk asymmetries lessened. This could be due to extreme drainage of plasma shrinking the size of the plasmasphere, particularly within the L-shells well below $-70°$ invariant latitude, while the stronger southern ionospheric outflow continued.

[15] The discoveries of the medium-to-high energy, tens of keV, O^+ abundant in the plasma sheet, LLBL, lobes and even their leakages into the magnetosheath [*Shelley et al.*, 1974; *Fritz and Wilken*, 1976; *Geiss et al.*, 1978; *Young*, 1979; *Candidi et al.*, 1982; *Seki et al.*, 1998; *Marcucci et al.*, 2004; *Chaston et al.*, 2005; *Ruan et al.*, 2005; *Bouhram et al.*, 2005] reveal the importance of heated ionospheric ions, which originate at tens of eV at the topside ionosphere. In some events, the flux of the O^+ in the morning side of LLBL was comparable with that of H^+ [*Chaston et al.*, 2005] and was much higher than that of the low-energy O^+ outflow leaving the ionospheric footpoint, observed by the FAST spacecraft, on the same flux tube. Statistical studies of keV ions at the geosynchronous orbit [*Lavraud et al.*, 2005] show that the keV O^+ to H^+ density ratio is maintained at $\sim$1.2 at the duskside, insensitive to the changes in the total ion density because of the sunward convection of the cold dense plasma in the plasma sheet at the peak of geomagnetic activity [e.g., *Terasawa et al.*, 1997]. This suggests that the O^+ abundance in the magnetosphere tends to maintain approximately a constant flux level, owing to the tenuous yet continuous supply from the polar ionosphere [*Liemohn et al.*, 2005], from one geomagnetic activity period to another, rather than regenerating completely at each activity

period, storm or substorm. In other words, there are mechanisms that heat and maintain O^+ at relatively constant energy and flux levels. The possible steady existence of low-energy O^+ in the magnetosphere on closed field lines might contribute locally and more directly to the source of higher-energy O^+ abundance. These low-energy O^+ could have come from the outer plasmasphere as an entrainment of the global magnetospheric convection [*Roberts et al.*, 1987]. Although our density moment estimates the total density of all ions, mostly H^+ and O^+ below 300 eV, the density distributions (Figure 4) have shown the persistence of high-density regions on closed field lines equatorward of the auroral regions (between the dashed curve pairs in each Figures 4a–4d) at all level of geomagnetic activity.

[16] The changing in the spatial distributions of the heating ratio (equation (3)) at various levels of geomagnetic activity (Figure 11) provides hints to physical processes that might occur in the magnetotail. At quiet time (Figure 11a), the ratio of heating was significantly larger than unity near the oval region at the midnight sector in the southern hemisphere but variable at higher latitudes in the northern hemisphere. At higher geomagnetic activity (Figures 11b and 11c), the regions of heating in the southern hemisphere broadened in local time and latitudes. The regions of heating in the northern hemisphere became localized at lower latitudes closer to the auroral oval region near the midnight sector. At extreme geomagnetic activity (Figure 11d), patches of hot regions, where the heating ratio $\mathrm{Log}_{10}(R_A) > 0.75$, are found to be prevalent, mostly around midnight near the auroral oval boundaries. This could be caused by patchy reconnections or current disruptions that heat the ions at discrete locations or times in the plasma sheet or plasma sheet boundary layers that map to the auroral regions. Studies of events selected from this period might help us to pinpoint the locations where the heating might occur. In general, regardless of processes that might heat the ions in the magnetotail, there is a persistent distribution of heated ions in the magnetotail. The seasonal effect is the most probable cause of the north–south asymmetry. When the Earth's dipole tilted toward the sun (Figure 6), the region of heating is more likely localized in the southern hemisphere as stronger cross-polar convection in the southern hemisphere occurs, except at extreme geomagnetic activity, when the asymmetry seems to disappear.

5. Conclusions

[17] On the basis of our statistical study of cold ion measurements from the Polar spacecraft in the near-Earth magnetotail, we find that the low-energy plasma, mostly of ionospheric origin, depends upon levels of geomagnetic activity, Sym-H, particularly the ion density, temperatures, parallel temperature asymmetric ratio, and convection. (1) Denser cold ions were observed at the dusk side ($N > 10\ \mathrm{cm}^{-3}$ compared with $1\ \mathrm{cm}^{-3}$ on average) - consistent with the formation of plasma plumes and enhanced bulge region formed as they wrapped under corotation. (2) Higher temperatures were observed in the auroral oval regions, and a larger temperature anisotropy ($T_{\parallel}/T_{\perp} > 2$ compared with 1.2 on average) was observed at the dawnside. (3) Heating processes were strongest near midnight and in the auroral oval regions, which mapped to PSBL or CPS, except during extremely high geomagnetic activity, when heating occurred at high latitudes toward the dawnside, which mapped to plasma mantle or distant magnetotail.

[18] **Acknowledgments.** The authors thank C.T. Russell of IGPP/UCLA for providing Polar magnetic field data, Space Physics Data Facility of NASA Goddard Space Flight Center for providing ACE plasma and magnetic field data, and Kyoto University World Data Center for providing Sym-H and Dst indices. This work was supported by the NASA Polar-Wind-Geotail project under WBS 889836.04.05.

[19] Amitava Bhattacharjee thanks Bengt Hultqvist and another reviewer for their assistance in evaluating this paper.

References

Boardsen, S. A., T. E. Eastman, T. Sotirelis, and J. L. Green (2000), An empirical model of the high-latitude magnetopause, *J. Geophys. Res.*, *105*(A10), 23,193–23,219.

Bouhram, M., B. Klecker, G. Paschmann, S. Haaland, H. Hasegawa, A. Blagau, H. Rème, J.-A. Sauvaud, L. M. Kistler, and A. Balogh (2005), Survey of energetic O^+ ions near the dayside mid-latitude magnetopause with cluster, *Ann. Geophys.*, *23*, 1281.

Candidi, M., S. Orsini, and V. Formisano (1982), The properties of ionospheric O^+ ions as observed in the magnetotail boundary layer and northern plasma lobe, *J. Geophys. Res.*, *87*(A11), 9097–9106.

Chappell, C. R., T. E. Moore, and J. H. Waite Jr. (1987), The ionosphere as a fully adequate source of plasma for the Earth's magnetosphere, *J. Geophys. Res.*, *92*(A6), 5896–5910.

Chaston, C. C., et al. (2005), Energy deposition by Alfvén waves into the dayside auroral oval: Cluster and FAST observations, *J. Geophys. Res.*, *110*, A02211, doi:10.1029/2004JA010483.

Chen, S.-H., and T. E. Moore (2004), Dayside flow bursts in the Earth's outer magnetosphere, *J. Geophys. Res.*, *109*, A03215, doi:10.1029/2003JA010007.

Chen, S.-H., and T. E. Moore (2006), Magnetospheric convection and thermal ions in the dayside outer magnetosphere, *J. Geophys. Res.*, *111*, A03215, doi:10.1029/2005JA011084.

Eastman, T. E., S. A. Boardsen, S.-H. Chen, S. F. Fung, and R. L. Kessel (2000), Configuration of high-latitude and high-altitude boundary layers, *J. Geophys. Res.*, *105*(A10), 23,221–23,238.

Farrugia, C. J., D. T. Young, J. Geiss, and H. Balsiger (1989), The composition, temperature, and density structure of cold ions in the quiet terrestrial plasmasphere: GEOS 1 results, *J. Geophys. Res.*, *94*(A9), 11,865–11,891.

Fritz, T. A., and B. Wilken (1976), Substorm generated fluxes of heavy ions at the geostationary orbit, in *Magnetospheric Particles and Fields*, edited by B. M. McCormac, p. 171, D. Reidel, Dordrecht, Netherlands.

Geiss, J., H. Balsiger, P. Eberhardt, H. P. Walker, L. Weber, D. T. Young, and H. Rosenbauer (1978), Dynamics of magnetospheric ion composition as observed by the GEOS mass spectrometer, *Space Sci. Rev.*, *22*(5), 537.

Goldstein, J., J. L. Burch, B. R. Sandel, S. B. Mende, P. C:son Brandt, and M. R. Hairston (2005), Coupled response of the inner magnetosphere and ionosphere on 17 April 2002, *J. Geophys. Res.*, *110*, A03205, doi:10.1029/2004JA010712.

Hammond, C. M., M. G. Kivelson, and R. J. Walker (1994), Imaging of the effect of dipole tilt on the magnetotail boundaries, *J. Geophys. Res.*, *99*(A4), 6079–6092.

Hirahara, M., T. Mukai, T. Terasawa, S. Machida, Y. Saito, T. Yamamoto, and S. Kokubun (1996), Cold dense ion flows with multiple components observed in the distant tail lobe by Geotail, *J. Geophys. Res.*, *101*(A4), 7769–7784.

Holzworth, R. H., and C.-I. Meng (1975), Mathematical representation of the auroral oval, *Geophys. Res. Lett.*, *2*(9), 377–380.

Iyemori, T. (1990), Storm-time magnetospheric currents inferred from mid-latitude geomagnetic field variations, *J. Geomagn. Geoelec.*, *42*, 1249–1265.

Iyemori, T., and D. R. K. Rao (1996), Decay of the Dst field of geomagnetic disturbance after substorm onset and its implication to storm-substorm relation, *Ann. Geophys.*, *14*, 608–618.

Lavraud, B., M. H. Denton, M. F. Thomsen, J. E. Borovsky, and R. H. W. Friedel (2005), Superposed epoch analysis of dense plasma access to geosynchronous orbit, *Ann. Geophys.*, *23*, 21,519–21,529.

Liemohn, M. W., T. E. Moore, P. D. Craven, W. Maddox, A. F. Nagy, and J. U. Kozyra (2005), Occurrence statistics of cold, streaming ions in the near-Earth magnetotail: Survey of Polar-TIDE observations, *J. Geophys. Res.*, *110*, A07211, doi:10.1029/2004JA010801.

Marcucci, M. F., et al. (2004), Energetic magnetospheric oxygen in the magnetosheath and its response to IMF orientation: Cluster observations, *J. Geophys. Res.*, *109*, A07203, doi:10.1029/2003JA010312.

Moore, T. E., et al. (1995), The thermal ion dynamics experiment and plasma source instrument, *Space Sci. Rev.*, *71*, 409.

Mukai, T., M. Hirahara, S. Machida, Y. Saito, T. Terasawa, and A. Nishida (1994), Geotail observation of cold ion streams in the medium distance magnetotail lobe in the course of a substorm, *Geophys. Res. Lett.*, *21*(11), 1023–1026.

Ohtani, S., P. C. Brandt, H. J. Singer, D. G. Mitchell, and E. C. Roelof (2006), Statistical characteristics of hydrogen and oxygen ENA emission from the storm-time ring current, *J. Geophys. Res.*, *111*, A06209, doi:10.1029/2005JA011201.

Roberts, W. T., Jr., J. L. Horwitz, R. H. Comfort, C. R. Chappell, J. H. Waite Jr., and J. L. Green (1987), Heavy ion density enhancements in the outer plasmasphere, *J. Geophys. Res.*, *92*(A12), 13,499–13,512.

Roux, A., S. Perraut, J. L. Rauch, C. de Villedary, G. Kremser, A. Korth, and D. T. Young (1982), Wave-particle interactions near Ω_{He+} observed on GEOS 1 and 2. II: Generation of ion cyclotron waves and heating of He^+ ions, *J. Geophys. Res.*, *87*(A10), 8174–8190.

Ruan, P., S. Y. Fu, Q.-G. Zong, Z. Y. Pu, X. Cao, W. L. Liu, X. Z. Zhou, and P. W. Daly (2005), Ion composition variations in the plasma sheet observed by Cluster/RAPID, *Geophys. Res. Lett.*, *32*, L01105, doi:10.1029/2004GL021266.

Russell, C. T., R. C. Snare, J. D. Means, D. Pierce, D. Dearborn, M. Larson, G. Barr, and G. Le (1995), The GGS/Polar magnetic fields investigation, in *The Global Geospace Mission*, edited by C. T. Russell, p. 563, Kluwer Acad., Norwell, Mass.

Seki, K., T. Terasawa, M. Hirahara, and T. Mukai (1998), Quantification of tailward cold O^+ beams in the lobe/mantle regions with Geotail data: Constraints on polar O^+ outflows, *J. Geophys. Res.*, *103*(A12), 29,371–29,382.

Shelley, E. G., R. G. Johnson, and R. D. Sharp (1974), Morphology of energetic O^+ in the magnetosphere, in *Magnetospheric Physics*, edited by B. M. McCormac, p. 135, D. Reidel, Dordrecht, Netherlands.

Sugiura, M., and D. J. Poros (1971), Hourly values of equatorial Dst for years 1957 to 1970, in *Rep. X-645-71-278*, Goddard Space Flight Center, Greenbelt, Md.

Terasawa, T., et al. (1997), Solar wind control of density and temperature in the near-Earth plasma sheet: WIND/GEOTAIL collaboration, *Geophys. Res. Lett.*, *24*(8), 935–938.

Trattner, K. J., S. M. Petrinec, W. K. Peterson, S. A. Fuselier, and H. Reme (2006), Tracing the location of the reconnection site from the northern and southern cusps, *J. Geophys. Res.*, *111*, A11211, doi:10.1029/2006JA011673.

Tsyganenko, N. A. (1995), Modeling the Earth's magnetospheric magnetic field confined within a realistic magnetopause, *J. Geophys. Res.*, *100*(A4), 5599–5612.

Wanliss, J. A., and K. M. Showalter (2006), High-resolution global storm index: Dst versus SYM-H, *J. Geophys. Res.*, *111*, A02202, doi:10.1029/2005JA011034.

Wilken, B., Q.-G. Zong, I. A. Daglis, Z. Y. Pu, S. Livi, T. Yamamoto, T. Doke, K. Maezawa, and S. Ullaland (1995), Tailward flowing energetic oxygen ion bursts associated with multiple flux ropes in the distant magnetotail: Geotail observations, *Geophys. Res. Lett.*, *22*(23), 3267–3270.

Young, D. T. (1979), Ion composition measurements in magnetospheric modeling, in *Quantitative Modeling of Magnetospheric Processes*, *Geophys. Monogr. Ser.*, *21*, edited by W. P. Olsen, p. 340, AGU, Washington, D. C.

Young, D. T., J. Geiss, H. Balsiger, P. Eberhardt, A. Ghielmetti, and H. Rosenbauer (1977), Discovery of He^{2+} and O^{2+} ions of terrestrial origin in the outer magnetosphere, *Geophys. Res. Lett.*, *4*(12), 561–564.

S.-H. Chen, Geospace Physics Laboratory, NASA Goddard Space Flight Center, Code 673, 8800 Greenbelt Rd, Greenbelt, MD 20771, USA. (sheng-hsien.chen@gsfc.nasa.gov)

T. E. Moore, Heliophysics Science Division, NASA Goddard Space Flight Center, Code 670, 8800 Greenbelt Rd, Greenbelt, MD 20771, USA.